that lends very strong credence to the theoretical ordering of these shift components. The smaller range in the σ_{33} data vs. the corresponding σ_{22} values can be readily interpreted in terms of the greater polarizability of the π electrons important in the σ_{22} term. As chemical shielding depends upon processes of electron excitation by the magnetic field, there will be a magnification effect due to the π electrons in variations in σ_{22} over that of the all σ-electron σ_{33} term. As the σ_{11} term is affected by the same π-electron excitation processes and would manifest similar magnification effects, then the much narrower σ_{11} range further argues for the conclusions made above regarding the similarity between the members of this series in the σ-π-electron mixing which would also be important in σ_{11}.

Unlike the data on the olefinic carbons, the tensor quantities for the methyl and methylene carbons cannot be even tentatively identified at the present time with specific orientation of the molecule in the magnetic field. This is because one does not have a model system such as ethylene upon which to compare the various shift components for the alkyl carbon shifts. Furthermore, except for one component in cyclopropene, the various methylene components are much closer together in value and as such the order of the shifts for the various geometric orientations may not even be preserved from compound to compound. This narrower range of shifts also would allow anisotropic, remote shielding terms to play a relatively more important role both in the overall aliphatic shift magnitudes and in the ultimate orientation of the principal axes of the shift tensor. For these reasons no attempt is made to rationalize the various aliphatic shielding components in terms of specific molecular structural features. It is sufficient to draw attention to the diversity of values observed in this study and to emphasize the ultimate importance such information may have in providing three-dimensional characterization of the electronic structure of molecules.

As the σ_{33} shift recorded for the methylene carbon in cyclopropene is sufficiently different, it does deserve some comment. This is especially the case since neither σ_{11} nor σ_{22} in cyclopropene are unusual when compared with the corresponding shifts in the other members of the series. Thus, it is seen that the anomalously high-field isotropic shift for the CH_2 in cyclopropene results from only one of the tensorial components appearing at a very high field. This observation provides a plausible explanation of the well-known high-field isotropic shifts recorded for this and other 3-membered rings.

In summary, ^{13}C tensorial shielding data for alkenes and cycloalkenes have been shown to provide a much richer source of structural information than the isotropic liquid shielding values. The information is directly related to the three-dimensional geometric and electronic structures of these molecules in such an intimate manner as to provide an interesting challenge for molecular quantum mechanic efforts at understanding small molecules.

Acknowledgment. This work was supported in part by the National Institutes of Health under Grant GM-08521-19 and by the National Science Foundation under Grant CHE7827094. We are grateful to Dr. R. Srinivasan (IBM Corp., Yorktown Heights, N.Y.) for *trans*-cyclooctene and to Mr. R. R. Clark for assistance in the preparation of cyclobutene.

Dynamics of the Primary Events in Bacterial Photosynthesis

Joshua Jortner

Contribution from the Department of Chemistry, Tel-Aviv University, Tel Aviv, Israel.
Received November 9, 1979

Abstract: This paper considers the primary light-induced electron-transfer (ET) processes in the reaction center of photosynthetic bacteria which involved ET from the electronically excited state of the bacteriochlorphyll *a* dimer $(BChl)_2$ to bacteriopheophytin (BPh) ((I.1)) and ET from BPh^- to ubiquinone (Q) ((I.2)). Ultrafast reactions I.1 and I.2, which are practically temperature independent over the range 4–300 K, cannot be accounted for in terms of low-temperature nuclear tunnelling through a nuclear barrier, as such a mechanism would imply an unrealistically high characteristic molecular frequency for the electron-donor and the electron-acceptor centers. Two mechanisms for ultrashort, temperature-independent processes I.1 and I.2 were examined. The rate of the ET reaction (I.2) is considerably longer than characteristic medium-induced vibrational relaxation rates, so that process I.2 has to occur from a thermally equilibrated nuclear configuration of BPh^-Q. Reaction I.2 is assigned to an activationless nonadiabatic ET process, the short lifetimes for this reaction stemming from a large value of the electronic coupling $V \simeq 4$ cm^{-1} which, according to rough estimates, implies that the average BPh^-Q spacing is ~ 10 Å. We propose that the ultrafast reaction (I.1) occurs from a nonequilibrium nuclear configuration of the $(BChl)_2$*BPh initially excited state which is located above the crossing point of the nuclear potential surfaces for $(BChl)_2$*BPh and for $(BChl)_2^+BPh^-$. Such a novel ET mechanism involves competition between ET and vibrational relaxation. A theory has been developed to handle this problem and applied to reaction I.1. A microscopic molecular scheme for the primary events of charge separation in bacterial photosynthesis is proposed, which rests on the optimization of (a) the intramolecular distortions of the equilibrium nuclear configurations (these nuclear distortions determine the vibrational overlap contributions to the ET rates) and (b) the intermolecular spatial organization of the donor and the acceptor (the donor–acceptor separation (and orientation) determines the electronic coupling which dominates the preexponential contribution to the ET rate). The molecular scheme is successful in accounting for the qualitative and the quantitative features of the primary ET rates and in providing a picture for the directionality, selectivity, and efficiency of the charge separation events.

I. Introduction

The understanding of the primary events in bacterial photosynthesis is of central importance for the elucidation of the basic mechanisms of the acquisition, storage, and disposal of energy in the photosynthetic process.[1] Photosynthetic bacteria, like green plants, contain an antenna system that transfers the excitation energy to the reaction center where charge separation occurs. By a suitable chemical treatment of the bacterial chromatophores the reaction center can be isolated from the antenna pigments.[2,3] During the last few years extensive new information on the dynamics of charge separation in such "isolated" reaction centers has emerged from experimental studies, utilizing the modern techniques of ultrafast picosecond spectroscopy.[4-11] Indeed, the

(1) (a) Dutton, P. F.; Prince, R. C.; Tiede, D. M.; Petty, K. M.; Kaufmann, K. J.; Netzel, T. L.; Rentzepis, P. M. *Brookhaven Symp. Biol.* **1976**, *28*, 213. (b) Dutton, P. L.; Leigh, J. S.; Prince, R. C.; Tiede, D. M. "Tunnelling in Biological Systems"; Academic Press: New York, 1979; p 319. (c) Dutton, P. L.; Prince, R. C.; Tiede, D. M. *Photochem. Photobiol.* **1978**, *28*, 939. (d) Holten, D.; Windsor, M. W. *Annu. Rev. Biophys. Bioeng.* **1978** *7*, 189.

(2) Clayton, R. K.; Wang, R. T. *Methods Enzymol.* **1971**, *23*, 696.

(3) Feher, G. *Photochem. Photobiol.* **1971**, *14*, 373.

0002-7863/80/1502-6676$01.00/0

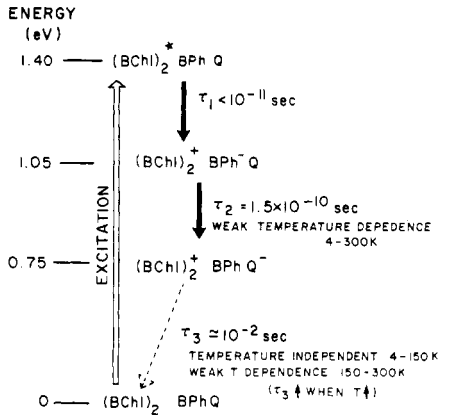

Figure 1. Energetics of the primary ET processes. Processes I.1 and I.2 involve primary charge separation, while reaction I.3 occurs in vitro in the absence of cytochrome reduction.

reaction center in bacterial photosynthesis is relatively simple and sufficiently well understood to serve as a basic model system for the application of new experimental methods and as a testing ground for novel theoretical ideas.

The reaction center particles of typical systems such as *Rhodopseudomonas spheroides* contain four molecules of bacteriochlorophyll *a* (BChl), two molecules of bacteriopheophytin (BPh), one ubiquinone-10 (Q), one nonheme iron atom, presumably associated with Q, and three proteins.[1] It is believed that the $(BChl)_2$ dimer, one BPh, and Q are involved in the primary charge-separation process.[1,12] Experimental studies utilizing the techniques of picosecond spectroscopy[4-11] have established that the sequence of primary processes of charge separation within the reaction center occurs on the subnanosecond time scale. In particular, it was demonstrated that the initial processes in the reaction center are as follows.

(A) Excitation.

$$(BChl)_2BPhQ \xrightarrow{h\nu} (BChl)_2{}^*BPhQ \qquad (I.0)$$

Ultrafast laser excitation of the bacterial reaction centers by mode-locked lasers was performed at 530 nm which is absorbed by BPh. However, as shown by Netzel et al.,[4] the 530-nm electronic excitation is transferred from BPh to $(BChl)_2$ on a time scale which is shorter than 10 ps.

(B.1) Primary Step of Charge Separation.

$$(BChl)_2{}^*BPhQ \xrightarrow{\tau_1} (BChl)_2{}^+BPh^-Q \qquad (I.1)$$

This first chemical process corresponds to electron transfer (ET) which is characterized by the following features: (1a) The lifetime τ_1, i.e., the reciprocal unimolecular rate, is ultrashort,[4-11] the primary process occurring on the picosecond time scale. Rentzepis and colleagues have shown[4-8,10] that τ_1 is shorter than 10 ps at room temperature. Parson et al.[11] have reported that $\tau_1 \simeq 3$ ps at 300 K. (1b) The upper limit for τ_1 is temperature independent over the temperature range 4-300 K.[10]

(B.2) Second Step of Charge Separation. This involved ET from BPh^- to Q (eq I.2).

$$(BChl)_2{}^+BPh^-Q \xrightarrow{\tau_2} (BChl)_2{}^+BPhQ^- \qquad (I.2)$$

Its features are as follows: (2a) The lifetime τ_2 is ~150 ps at 300 K. (2b) τ_2 exhibits very weak temperature dependence over the temperature range 4–300 K.[10,11] Peters et al. have observed[10] that τ_2 is practically identical at 300 and 4 K, while Parson et al.[11] have reported that τ_2 decreases about twofold by going from 300 to 83 K.

Figure 1 portrays the relevant energetics for the primary processes.[1] The energies of the neutral ground state $(BChl)_2BPhQ$ and of the electronic ground-state ionic systems $(BChl)_2{}^+BPh^-Q$ and $(BChl)_2{}^+BPhQ^-$ correspond to the equilibrium nuclear configuration, while the energy of the electronically excited state $(BChl)_2{}^*BPhQ$ corresponds to a vertical excitation relative to the neutral ground state $(BChl)_2BPhQ$, which is achieved either by direct photon absorption or by ultrafast electronic energy transfer. We have also denoted in Figure 1 the relevant ET processes. Here we have also included the back-reaction involving charge recombination, occurring in the reaction center in the absence of cytochrome reduction:[1,13,14]

$$(BChl)_2{}^+BPhQ^- \xrightarrow{\tau_3} (BChl)_2BPhQ \qquad (I.3)$$

The characteristics of reaction I.3 are as follows: (3a) The process is characterized by the very slow lifetime τ_3, $\sim 10^{-2}$/s. (3b) τ_3 exhibits only a very weak temperature dependence over the temperature range 4–300 K. The lifetime is temperature independent over the range 4–150 K, while in the temperature range 150–300 K the lifetime τ_3 increases with increasing temperature, the lifetime at 300 K being longer by a numerical factor of ~3–4 relative to that at 150 K.

II. Aims and Claims

A comprehensive theory of the dynamics of charge separation within the reaction center in bacterial photosynthesis has to provide a proper physical picture for the following unique characteristics of this system.

(1) Absolute reaction rates: primary processes (I.1) and (I.2) are ultrafast,[4-11] providing some of the examples of the fastest ET processes recorded up to date. On the other hand, the recombination reaction (I.3) (exhibited only in the absence of cytochrome *c*) is quite slow. A comprehensive theory has to provide adequate interpretation for the variation of the ET rates over 10 orders of magnitude.

(2) Temperature dependence of the rates:[10] the rates for ultrafast processes I.1 and I.2, as well as for the slow process (I.3), are weakly temperature dependent over a broad temperature range. This weak temperature dependence drastically differs from the characteristics of the celebrated DeVault–Chance reaction[15] which involved ET from cytochrome *c* to the reaction center, exhibiting a marked temperature dependence over the range 100–300 K and revealing the features of temperature independent nuclear tunnelling at low ($T < 100$ K) temperatures.[15-20] In addition, it is intriguing to note that the weak temperature dependence of reaction I.3 and possibly also of reaction I.2 is manifested in a decrease of the rates with increasing temperature; i.e., these reactions are retarded at high temperatures, in contrast to the

(4) Netzel, T. L.; Rentzepis, P. M.; Leigh, J. S. *Science (N.Y.)* **1973**, *18*, 238.
(5) Kaufmann, K. J.; Dutton, P. J.; Netzel, T. L.; Leigh, J. S.; Rentzepis, P. M. *Science (Washington, D.C.)* **1975**, *188*, 1301.
(6) Kaufmann, K. J.; Petty, K. M.; Dutton, P. L.; Rentzepis, P. M. *Biochem. Biophys. Res. Commun.* **1976**, *70*, 839.
(7) Leigh, J. S.; Netzel, T. L.; Dutton, P. L.; Rentzepis, P. M. *FEBS Lett.* **1974**, *48*, 136.
(8) Netzel, T. L.; Rentzepis, P. M.; Tiede, D. M.; Prince, R. C.; Dutton, P. L. *Biochim. Biophys. Acta* **1977**, *460*, 467.
(9) Rockley, M. G.; Windsor, M. W.; Cogdell, R. J.; Parson, W. U. *Proc. Natl. Acad. Sci. U.S.A.* **1975**, *72*, 2251.
(10) Peters, K.; Avouris, Ph.; Rentzepis, P. M. *Biophys. J.* **1978**, *23*, 207.
(11) Parson, W. W.; Schenck, C. C.; Blankenship, R. E.; Holten, D.; Windsor, M. W.; Shank, C. V. "Frontiers of Biological Energetics"; Academic Press: New York, 1978; Vol. I, p 37.
(12) Dutton, P. L.; Petty, K. M.; Bonner, H. S.; Morse, S. D. *Biochim. Biophys. Acta* **1975**, *387*, 536.
(13) Parson, W. W. *Annu. Rev. Microbiol.* **1974**, *28*, 41.
(14) Hoff, A. J. *Phys. Rep.* **1979**, *54*, 75.
(15) DeVault, D.; Chance, B. *Biophys. J.* **1966**, *6*, 825.
(16) Hopfield, J. J. *Proc. Natl. Acad. Sci. U.S.A.* **1974**, *71*, 3640.
(17) Jortner, J. *J. Chem. Phys.* **1976**, *64*, 4860.
(18) (a) Hopfield, J. J. In "Electrical Phenomena at the Biological Membrane Level"; Elsevier: Amsterdam, 1977. (b) Hopfield, J. J. In "Tunnelling in Biological Systems"; Academic Press: New York, 1979.
(19) Kuznetsov, A. M.; Søndergard, N. C.; Ulstrup, J. *Chem. Phys.* **1978**, *29*, 383.
(20) Buhks, E.; Bixon, M.; Jortner, J. *Chem. Phys.*, in press.

common universal features of chemical reactions.

(3) Directionality of the overall charge-separation processes: the charge-separation process proceeds "downhill" on the energy ladder (see Figure 1) and the reverse "uphill" processes (II.1′) and (II.2′)

$$(BChl)_2{}^+BPh^-Q \xrightarrow{\tau_{1'}} (BChl)_2{}^*BPhQ \qquad (II.1')$$

$$(BChl)_2{}^+BPhQ^- \xrightarrow{\tau_{2'}} (BChl)_2{}^+BPh^-Q \qquad (II.2')$$

are slow on the relevant time scale. From the experimental data for processes I.2 and I.3 we can assert that $\tau_{1'} \gg \tau_2 \approx 10^{-10}$ s, while $\tau_{2'}$ is slow on the time scale of τ_2.

(4) Specificity of the route of the charge-separation process: the charge separation occurs in the ultrafast sequence of process I.1 followed by process I.2, while the "shortcuts" such as eq II.4

$$(BChl)_2{}^*BPhQ \xrightarrow{\tau_4} (BChl)_2{}^+BPhQ^- \qquad (II.4)$$

are inefficient, e.g., $\tau_4 \gg 10^{-11}$

(5) Inefficiency of charge recombination: the only recombination process (I.3) (exhibited in the absence of cytochrome reduction) is very inefficient. The "downhill" charge-recombination process (II.5)

$$(BChl)_2{}^+BPh^-Q \xrightarrow{\tau_5} (BChl)_2BPhQ \qquad (II.5)$$

is slow so that it cannot compete with process I.2, i.e., $\tau_5 \gg 10^{-10}$.

(6) Inefficiency of the intramolecular radiationless deactivation process (II.6),

$$(BChl)_2{}^*BPhQ \xrightarrow{\tau_6} (BChl)_2BPhQ \qquad (II.6)$$

which represents a conventional radiationless transition to the ground state in a large molecule has to be ensured by the condition $\tau_6 \gg 10^{-11}$ s, or otherwise the efficiency of the charge separation will be reduced. The low-lying singlet excited state of the $(BChl)_2$ dimer located at 1.4 eV can exhibit, in principle, a fast radiationless process, as is the case for the first singlet state of azulene[21] which decays radiationlessly to the ground state on the picosecond time scale.

There has been considerable theoretical activity aimed toward the understanding of ET in bacterial photosynthesis.[16-20] Hopfield has recently applied[18] his semiclassical model[16] for charge separation in bacterial photosynthesis. By a proper choice of the nuclear distortions, which determine the nuclear contribution to the ET rate, i.e., a state of affairs subsequently referred to by us as an activationless ET, Hopfield[18] was able to account for the temperature independence of the charge-recombination process (I.3). However, Hopfield's physical parameters[18] predict quite substantial activation energies for processes I.1 and I.2 in contrast to the experimental facts.[11] We would like to address the question whether conventional ET theory,[16-27] with an appropriate choice of the electronic and nuclear parameters, is adequate or whether new concepts and ideas have to be invoked for the understanding of the primary charge-separation processes in bacterial photosynthesis. In the present paper an attempt is made to provide an overall description of the overall charge-separation process in bacterial photosynthesis by proposing that intramolecular and intermolecular organization results in the optimization of nuclear configurational changes and the intermolecular spacings, which determine the electronic coupling accompanying the sequence of ET reactions, can account for the qualitative and quantitative features of the rates, as well as for the directionality and the efficiency of the overall charge-separation process. In section III, we shall introduce a criterion for the applicability of conventional ET theory in condensed phases, which rests on the feasibility of the separation of time scales for vibrational relaxation and for ET. On the basis of this criterion we shall argue that the fast, subnanosecond charge separation reaction (I.2), as well as other temperature-independent processes such as reaction I.3, involve an activationless ET process, which can be accounted for in terms of conventional nonadiabatic multiphonon theory[16-26] for specific nuclear distortions. This idea of activationless ET in biological systems was proposed by Hopfield[18] for the slow recombination process (I.3), while several groups[11,22,23] have considered recently the possibility that reaction I.2 occurs via an activationless mechanism. In section IV, we shall advance a detailed theory of activationless ET, which accounts for the temperature independence over a wide range and which predicts a small negative apparent activation energy at high temperatures. A detailed analysis of the second charge-separation process (I.2) in terms of an activationless ET process will then be provided. Concerning the primary charge-separation reaction (I.1), we shall propose in section V that the ultrafast picosecond initial ET process occurs at a crossing point of two nuclear potential surfaces, being so efficient that the system did not reach thermal equilibrium.[24] To account for this process, one has to go beyond the theory of conventional ET reactions. On the basis of those ideas pertaining to primary ET from a nonequilibrium nuclear configuration and to subsequent activationless process from thermally equilibrated nuclear manifolds, a reasonable description will emerge for the biological utilization of energy in the bacterial photosynthetic center.

III. Conventional Theory of ET in Biological Systems

ET processes in biological systems were described[16,17] in terms of nonadiabatic multiphonon radiationless transitions. This physical picture bears a close analogy to the Marcus–Levich theory of outer-sphere ET between ions in solution. However, for ET in biological systems nuclear distortions of high-frequency vibrational modes are crucial in determining the dynamics of the process,[16,17] while for ET in inorganic systems a major contribution to the rate originates from long-range, low-frequency polarization interactions.[25,26] We shall proceed to discuss briefly the theory of nonadiabatic ET, not in order to rehash well-known results[16-26] but rather to establish the time scale for the validity of the conventional theory and to explore its technical and conceptual extensions.

The entire electronic nuclear system can be adequately characterized by the two distinct zero-order electronic states a ≡ DA, corresponding to the donor (D)–acceptor (A) pair, and b ≡ D^+A^-, representing the reduced state of the acceptor, together with the oxidized state of the donor. For each of these two electronic states one can construct a multidimensional potential surface $U_{DA}(\vec{q})$ and $U_{D^+A^-}(\vec{q})$ determined by the set $\{\vec{q}\}$ of the nuclear displacement of the entire system. Subsequently, one can construct the vibronic levels $\{|av\rangle\}$ and $\{|bw\rangle\}$ corresponding to the nuclear potential surfaces DA and D^+A^-, respectively. Here v and w denote the true vibrational levels. The nonadiabatic ET process should be envisioned in terms of a nonradiative transition occurring in a supermolecule which consists of the donor–acceptor and the entire medium. The ET process involves the transitions $|av\rangle \rightarrow \{|bw\rangle\}$ from an initial state $|av\rangle$ to the manifold $\{|bw\rangle\}$ which is quasi-degenerate with it. The microscopic rate constant W_{av} for a transition $|av\rangle \rightarrow \{|bw\rangle\}$ can be described in terms of the nonadiabatic formulation provided that the "residual" electronic coupling is weak relative to the characteristic vibrational energies of the system. In the nonadiabatic limit the microscopic ET rate is

$$W_{av} = \frac{2\pi}{\hbar}|V|^2 \sum_w |f_{bw,av}|^2 \delta(E_{bw} - E_{av}) \qquad (III.1)$$

where $f_{bw,av}$ is the vibrational overlap integral between the nuclear wave function of the states $|av\rangle$ and $|bw\rangle$, while E_{bw} and E_{av}

(21) Huppert, D.; Jortner, J.; Rentzepis, P. M. *Isr. J. Chem.* **1972**, *16*, 277.
(22) Sarai, A. *Chem. Phys. Lett.* **1979**, *63*, 360.
(23) (a) Jortner, J., paper presented at the ISOX-III Conference, June 1979, Albany, New York, U.S.A. (b) Buhks, E.; Jortner, J. *FEBS Lett.* **1980**, *109*, 117.
(24) Jortner, J. *Philos. Mag.* **1979**, *B40*, 317.
(25) Levich, V. *Adv. Electrochem. Electrochem. Eng.* **1966**, *4*, 249.
(26) Kestner, N. R.; Logan, J.; Jortner, J. *J. Phys. Chem.* **1974**, *78*, 2178.
(27) Marcus, R. A. *Annu. Rev. Phys. Chem.* **1964**, *15*, 155.

represent the energies of those vibronic states. V represents the electronic coupling corresponding to the residual one-electron two-center exchange interaction between D and A, which are spatially fixed at the separation R. The δ function in eq III.1 ensures energy conservation.

In order to derive a macroscopic ET rate expression, we have to invoke the central assumption of separation of time scales for vibrational relaxation and for ET. The electron dronor and the electron acceptor are coupled to a phonon bath of the entire media. Medium-induced vibrational relaxation (VR) and vibrational excitation are fast on the time scale of the microscopic rates W_{av} for ET, i.e.

$$W_{av} \ll \gamma_{VR} \tag{III.2}$$

where γ_{VR} represents a typical medium-induced VR rate. Such VR times of optical phonons, due to anharmonic coupling, were experimentally interrogated by using the methods of picosecond spectroscopy, typical values being $\gamma_{VR}^{-1} \approx 5 \times 10^{-12}$ s.[28-30] In the conventional description of ET processes the assumption of fast VR is taken for granted. Provided that VR is "fast", according to eq III.2, the experimental ET rate $W_{a\to b}$ from the initial electronic state of the donor (D)–acceptor (A) pair $|a\rangle \equiv$ DA to the final electronic state $|b\rangle \equiv D^+A^-$ can be expressed in terms of a thermal average of the microscopic rates, the averaging being taken over the manifold $\{|av\rangle\}$ of the initial states:

$$W_{a\to b} = \sum_v p_v W_{av} \tag{III.3}$$

where the thermal population of the $|av\rangle$ level is

$$p_v = \exp(-E_{av}/k_B T)/Z_I \tag{III.4a}$$

and

$$Z_I = \sum_v \exp(-E_{av}/k_B T) \tag{III.4b}$$

denotes the partition function of the DA manifold. Armed with eq III.1, III.3, and III.4a we obtain the conventional ET rate in the final form

$$W_{a\to b} = \frac{2\pi}{\hbar}|V|^2 F \tag{III.5}$$

where

$$F = \sum_v \sum_w p_v |f_{av,bw}|^2 \delta(E_{bw} - E_{av}) \tag{III.6}$$

is the thermally averaged nuclear Franck–Condon factor.

The various aspects of intermolecular organization which determine the electronic and nuclear constituents to the ET process are now apparent from a cursory examination of eq III.5. The nonadiabatic multiphonon rate constant in eq III.5 is expressed as a product of the electronic coupling V, and the thermally averaged Franck–Condon nuclear vibrational overlap factor F in eq III.6. The spatial orientations and the spacing R of the donor–acceptor pair determines the electronic contribution V. Reliable numerical calculations were performed for V for the case of electron transfer between aromatic molecules which rest on many electron calculations incorporating intermolecular exchange and properly accounts for the behavior of the tails of the electronic wave functions.[31,32] For the molecular crystals like naphthalene or anthracene, the electronic dependence of these two-center one-electron transfer integrals, V, on the intermolecular separation R can be faithfully reproduced by an exponential dependence, which is in accord with previous semiquantitative proposals.[16,17] In our analysis of the V dependence of R, the intermolecular donor–acceptor separation was specified in terms of the distance

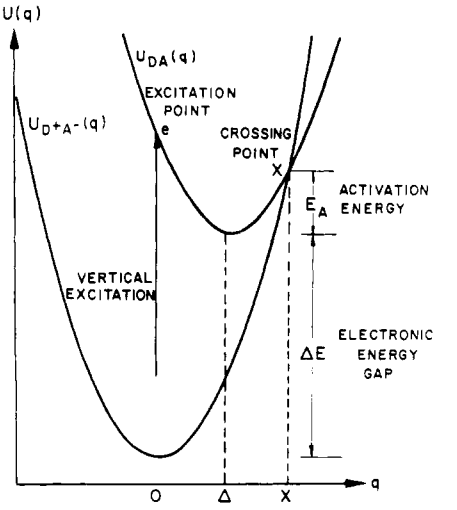

Figure 2. One-dimensional nuclear configurational diagram for ET.

between the centers of the two aromatic molecules rather than by the edge-to-edge spacing. The distance dependence of V is affected also by the relative orientation of the donor–acceptor pair. This angular dependence of V has not yet been considered and may be of considerable importance in determining the magnitude of the electronic coupling. In what follows we shall consider only the distance dependence of V, which rests on quantum mechanical calculations[31] of the two-center one-electron integral between parallel aromatic molecules. For a pair of parallel aromatic molecules A^-A, where A denotes naphthalene or anthracene, the numerical results[31] for the electronic coupling V can be expressed in the analytical form

$$V = V_0 e^{-\alpha R} \tag{III.7}$$

with

$$V_0 = 1.0 \times 10^5 \text{ cm}^{-1} \qquad \alpha = 1.0 \text{ Å}^{-1} \tag{III.7a}$$

Equation III.7 will be adopted to account for the electronic coupling V which determines the magnitude of the ET rate. The nuclear contribution F (eq III.6) to the ET rate depends explicitly on two types of modes, i.e., the low-frequency polar phonon modes of the medium- and high-frequency molecular modes of the D and A centers. From the point of view of general methodology, the coupling with the medium modes is crucial to ensure the irreversibility of the ET process. However, when the coupling with the molecular modes dominates, one can get away with neglecting the explicit contribution of the medium modes and adopting a coarse-graining procedure for the contribution of the molecular modes. For the DeVault–Chance ET reaction[15] the nuclear reorganization energy due to the coupling with the molecular vibrations exceeds by about 1 order of magnitude the nuclear organization energy originating from the coupling with medium phonons.[16-20] This suggests that in the photosynthetic center the coupling with molecular vibrations dominates the nuclear contribution to the ET dynamics. In view of our current ignorance regarding the nature of these molecular vibrations, we shall subsum the contributions of all these modes into a single molecular vibration of average frequency, ω, and a (large) coupling strength, Δ. The result for the ET rate (eq III.5) obtained from such a single-frequency model system has to be coarse grained over a finite energy range.[17] Such coarse graining accounts implicitly for the effects of the dispersion of weakly coupled medium modes and for vibrational relaxation of molecular modes.[17] This averaging procedure will erode all nonphysical resonance effects exhibited in the mathematical treatment of the single-mode model. To proceed with the single-mode approximation, we shall adopt a grossly over-simplified description of the nuclear potential surfaces in terms of a simple configurational diagram (Figure 2) consisting of one-dimensional potential surfaces:

$$U_{DA}(q) = (\hbar\omega/2)q^2 \tag{III.8}$$

(28) Laubereau, A.; Von Der Linde, D.; Kaiser, W. *Phys. Rev. Lett.* **1971**, *27*, 802.
(29) Laubereau, A.; Wochner, G.; Kaiser, W. *Opt. Commun.* **1975**, *14*, 175.
(30) Alfano, R. R.; Shapiro, S. L. *Phys. Rev. Lett.* **1971**, *26*, 1247.
(31) Jortner, J.; Rice, S. A. In "Physics of Solids at High Pressures"; Tomizuka, C. T., Emrich, R. M., Eds.; Academic Press: New York, 1975; p 63.
(32) See, for example, ref 17.

$$U_{D^+A^-}(q) = (\hbar\omega/2)(q - \Delta)^2 + \Delta E \qquad \text{(III.8a)}$$

The single nuclear coordinate q is expressed in terms of reduced dimensionless units normalized to the root-mean-square displacement of the zero-point motion. Δ is the (reduced) horizontal displacement of the minima of the two potential surfaces. ΔE is the electronic energy gap representing the vertical displacement of the minima of the potential surfaces. The electron-vibration coupling is

$$S = \Delta^2/2 \qquad \text{(III.9)}$$

being characterized by the coupling energy

$$E_s = S\hbar\omega \qquad \text{(III.9a)}$$

The ET rate (eq III.5) can be expressed in the well-known form[17]

$$W = A \exp[-S(2\bar{v} + 1)] I_p\{2S[\bar{v}(\bar{v} + 1)]^{1/2}\}[(\bar{v} + 1)/\bar{v}]^{p/2} \qquad \text{(III.10)}$$

where $I_p\{\cdot\}$ stands for the modified Bessel function of order p. The electronic coupling is

$$A = 2\pi|V|^2/\hbar^2\omega \qquad \text{(III.11a)}$$

the reduced energy gap being

$$p = |\Delta E|/\hbar\omega \qquad \text{(III.11b)}$$

while the temperature dependence is incorporated with the Bose factor

$$\bar{v} = [\exp(\hbar\omega/k_BT) - 1]^{-1} \qquad \text{(III.11c)}$$

The simple ET rate expression (III.10) holds for both exoergic ($\Delta E < 0$) and endoergic ($\Delta E > 0$) processes. For endoergic processes the rate is activated at all temperatures. For exoergic processes the ET rate (eq III.10) exhibits a continuous transition from a low-temperature nuclear tunnelling (see eq III.12), which is determined by Poissonian nuclear overlap integral, to a high-temperature activated rate expression, eq III.13, where the activation energy E_A is given by the quadratic function (III.14).

$$W = A \exp(-S)\frac{S^p}{p!}; \quad k_BT \ll \hbar\omega \qquad \text{(III.12)}$$

$$W = A\left(\frac{\hbar\omega}{4\pi S k_BT}\right)^{1/2} \exp[-E_A/k_BT]; \quad k_BT \gg \hbar\omega \qquad \text{(III.13)}$$

$$E_A = (\Delta E + S\hbar\omega)^2/4S\hbar\omega \qquad \text{(III.14)}$$

Equation III.10, together with its limiting situations given by eq III.12 and III.13, constitute a reasonable description for the ET dynamics of exoergic reactions in a system where nuclear distortions are essentially determined by one type of vibrational modes, which in the present case correspond to molecular vibrations of the local donor and acceptor centers.

The conventional theory of ET for exoergic processes predicts a low-temperature rate, which is temperature independent. The cardinal question we should consider is whether the ultrafast primary step (I.1) as well as the second step (I.2) of charge separation can be interpreted in terms of exoergic reactions characterized by temperature-independent tunnelling according to eq III.12. To answer this question, we have to provide a more accurate estimate of the "transition temperature" T_0 from low-temperature nuclear tunnelling to the high-temperature activated region. This problem was considered originally by Goldanskii.[33] It can also be handled within the framework of the multiphonon formalism. The low-temperature rate for exoergic processes can be obtained from eq III.12 by the use of the Stirling approximation.

$$W = A \exp(-S) \exp(-\gamma p)/(2\pi p)^{1/2} \qquad \text{(III.15)}$$

$$\gamma = \ln(p/S) - 1$$

(33) Goldanskii, V. I. *Dokl. Acad. Nauk USSR* **1959**, *124*, 1261; **1959**, *127*, 1037.

Equation III.15 represents the energy gap law (EGL) for exoergic ET processes, which is analogous to the EGL for intramolecular electronic radiationless transitions. On the other hand, the activation energy (eq III.14) at high temperatures takes the form of eq III.14a.

$$E_A = \hbar\omega(p - S)^2/4S \qquad \text{(III.14a)}$$

We look now for the temperature T_0 where the ET rates given by eq III.15 and by eq III.13 and III.14a are equal. The temperature T_0 which marks the onset of the T dependence of W is roughly given by the condition (III.16).

$$k_BT_0 \simeq \hbar\omega(p - S)^2/4S(S + \gamma p) \qquad \text{(III.16)}$$

Condition III.16 is applicable for a broad range of the parameters p and S, excluding the special case $p = S$ which will be considered in section IV. Two limiting conditions of eq III.16 are of interest. In the strong electron-vibrational coupling situation (Figure 4) $S \gg 1$. One can also expect that $S > p$, whereupon $k_BT_0 \approx \hbar\omega/4$. In the weak electron-vibrational coupling situation $S \leq 1$, $p > S$, and $k_BT_0 \approx (\hbar\omega/4)(p/S\gamma)$ and as now $\gamma > 1$, we expect again that $k_BT_0 \approx \hbar\omega/4$.

Attempting to interpret processes I.1 and I.2 in terms of conventional exoergic ET processes, which at low T exhibit tunnelling through a barrier while at high T are characterized by a finite activation energy, i.e., $E_A > 0$, requires that for these processes $T_0 > 300$ K so that $\hbar\omega > 1000$ cm^{-1}. Thus, the characteristic molecular frequency of the donor and acceptor centers, which is expected to undergo substantial configurational distortion during the ET process, must exceed 1000 cm^{-1}. The detailed analysis[16,17,20] of the DeVault–Chance ET reaction[15] resulted in a much lower characteristic frequency of 350–450 cm^{-1}. We can safely assert that the characteristic frequency $\hbar\omega > 1000$ cm^{-1} is definitely too high so that reactions I.1 and I.2 cannot be explained on the basis of low-temperature nuclear tunnelling.

We would like to point out that the same considerations are applicable to the analysis of the slow temperature-independent recombination process (I.3), which again can be explained in terms of conventional low temperature only provided that $\hbar\omega$ is very high, again $\hbar\omega > 1000$ cm^{-1}. It should be noted that the "transition" temperature T_0 is determined by the nuclear contribution to the rate, while the absolute value of W is also determined by the electronic coupling.

From the foregoing discussion it is apparent that the conventional rate expression of the exoergic ET process is inapplicable to reactions I.1 and I.2, as well as for the back-reaction (I.3). At this stage we should address ourselves to the question of whether the "conventional" nonadiabatic multiphonon nonradiative formalism, which results in the general ET rate (eq III.6), is applicable for the initial fast charge-separation processes. A central diagnostic criterion for the applicability of the conventional ET formalism involves condition III.2 for fast vibrational relaxation on the time scale of the ET process. As far as the ultrafast primary reaction (I.1) is concerned, we cannot be certain whether condition III.2 applies, and in section V we shall attempt to consider the possibility of going beyond conventional ET theory for the understanding of reaction I.1. As far as reaction I.2 is concerned, we can safely assert that $\tau_2 = 150$ ps $\gg \gamma_{VR}^{-1} \approx 1$–10 ps, whereupon the conditions for thermal equilibration are well satisfied. Needless to say, the slow recombination reaction (I.3) must proceed from a thermally equilibrated nuclear manifold.[18] We shall now proceed to examine the possibility that reaction I.2 as well as process I.3 can be described within the framework of conventional ET theory outlined above. However, these two reactions are characterized by unique characteristics of the intramolecular nuclear distortions which accompany the configurational changes involved in these ET processes.

IV. Activationless Electron Transfer

When the nuclear potential surfaces of the initial and the final electronic states involved in the nonadiabatic process cross at the minimum of the initial state, the conventional ET process is activationless or barrierless. The activationless ET process can be

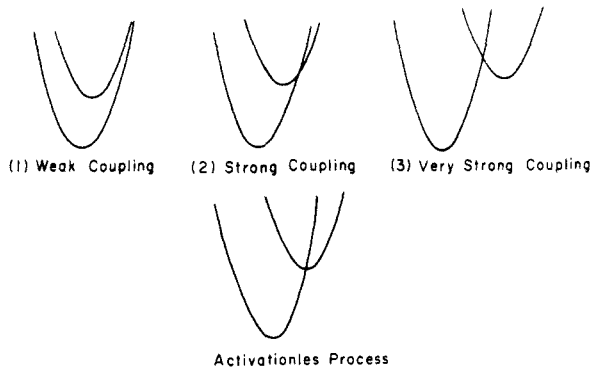

Figure 3. Nuclear coupling schemes for ET. The activationless exoergic process corresponds to the borderline case between the strong coupling and the very strong coupling situations.

characterized by two conditions. First, it is exoergic ($\Delta E < 0$). Second, the intramolecular nuclear distortions of the equilibrium configurations accompanying the ET process satisfy the condition (IV.17),

$$E_S = -\Delta E \qquad \text{(IV.17)}$$

which for our simple one-dimensional configurational diagram (see Figure 3) implies that $p = S$. It is now immediately apparent from eq III.14a that $E_A = 0$. Furthermore, examination of the low-temperature nuclear tunnelling rate (eq III.12 and III.14) reveals that $\gamma = 0$, so that the low-temperature rate is

$$W = A/(2\pi p)^{1/2} \quad k_B T \ll \hbar\omega \qquad \text{(IV.18)}$$

while the high-temperature rate is given by eq IV.19.

$$W = A(\hbar\omega/4\pi S k_B T)^{1/2} \quad k_B T \gg \hbar\omega \qquad \text{(IV.19)}$$

The following characteristics of the activationless ET processes should be emphasized: (1) The low-temperature, temperature-independent, rate manifests nonadiabatic ET, occurring from the lowest vibrational level of the initial potential surface. (2) The low-temperature rate in activationless processes (eq IV.19) essentially provides a determination of the electronic coupling V. (3) The high-temperature rate (eq IV.19), which reveals the temperature dependence $W \propto 1/T^{1/2}$, decreases with increasing T, thus exhibiting a negative apparent activation. From the mechanical point of view the $T^{1/2}$ term appearing in the denominator of eq IV.19 can easily be traced to the contribution from the partition function (eq III.4b). From the physical point of view, the retardation of the ET rate with increasing temperature can readily be rationalized. The fastest microscopic ET process occurs from the vibrationless level of the initial potential surface at the crossing of the final potential surface, while thermal excitation results in population of high vibration levels which are characterized by slower microscopic ET rates. (4) The temperature $\bar{T}_0$, which characterizes the "transition" from the temperature-independent region to the range specified by the negative apparent activation energy for activationless processes, is $k_B\bar{T}_0 \simeq \hbar\omega/2$, being again just determined by the nuclear contributions and not by the electronic coupling.

The second process reaction (I.2) in the sequence of charge separation with $\tau_2 = 150$ ps, as well as the recombination reaction (I.3) with $\tau_3 = 10$ ms, are assigned to activationless ET reactions and will be analyzed in terms of eq IV.18 and IV.19. We shall address two features of these processes, which pertain to the details of the temperature dependence and to the absolute values of the ET rates.

Consider first the qualitative features of the temperature dependence of activationless processes I.2 and I.3. The theory predicts a temperature-independent rate for $T < \bar{T}_0 = \hbar\omega/2k_B$, followed by a weak decrease of the rate with increasing temperature at $T > \bar{T}_0$. The temperature independence of reaction I.2 between cryogenic temperatures up to room temperature[10] is consistent with its assignment to an activationless process. The theory of activationless process quite properly accounts for the slight retardation of the rate of reaction I.2 with increasing temperature[11] and with τ_2 decreasing by a numerical factor of ~ 2 at 83 K relative to 300 K. Taking $\bar{T}_0 \simeq 150$ K, we expect τ_2 to decrease by a numerical factor of 1.4 over that temperature range. The rate of the back-reaction (I.3) is temperature independent over the range 4–150 K and subsequently reveals a decrease by a numerical factor of 3–4 with increasing temperature from 150–300 K.[13,14,34] The negative apparent activation energy of reaction I.3 is qualitatively consistent with the theory of activationless processes outlined herein. The $1/T^{1/2}$ temperature dependence expected from the nuclear contribution to the rate results in a decrease of the rate by a numerical factor of 1.4 over the temperature range 150–300 K, which is lower than the experimental value. An additional effect, which results in the slight retardation of the rate with increasing temperature, may originate from thermal expansion effects[14] which in turn result in the increase of the donor–acceptor spacing R and, consequently, in the decrease of the electronic coupling with increasing temperature.

Next, we consider the absolute rates of reactions I.2 and I.3. The low-temperature rate of an activationless process (eq IV.18) is

$$W = 4.7 \times 10^{11}|V/\text{cm}^{-1}|^2/(\hbar\omega/\text{cm}^{-1})p^{1/2}\ \text{s}^{-1} \qquad \text{(IV.20)}$$

which for typical parameters $\hbar\omega = 400$ cm^{-1} and $\Delta E = 2400$ cm^{-1} results in $W = 5 \times 10^8|V/\text{cm}^{-1}|^2$ s^{-1}. Utilization of the experimental data for τ_2 or τ_3, together with eq III.7, results in $V \simeq 4$ cm^{-1} and donor–acceptor spacing of $R \simeq 10$ Å for the charge-separation reaction (I.2). For the back-recombination reaction (I.3) occurring in vitro, $V \simeq 5 \times 10^{-4}$ cm^{-1}, in accordance with Hopfield's result,[18] which according to relation III.7 leads to a donor–acceptor separation of $R \simeq 20$ Å. From this analysis it is apparent how intramolecular configurational changes, as well as intermolecular donor–acceptor organization, optimize the activationless forward process (I.2) and block the back-reaction (I.3). The intramolecular nuclear displacements accompanying ET are optimal for both the desirable process (I.2) as well as for the undesirable back-reaction (I.3). On the other hand, close proximity of the $(BChl)_2$ and the BPh makes the secondary charge-separation process (I.2) very efficient due to large electronic coupling, while the large $(BChl)_2Q^-$ spacing results in exceedingly small electronic coupling making the back-process (I.3) ineffective.

V. Competition between Electron Transfer and Vibrational Relaxation

(A) The Primary ET Process. The ultrafast primary charge-separation process (I.1) with $\tau_1 \leq 10^{-11}$ s over the temperature range 4–300 K cannot be assigned to a conventional exoergic ET characterized by a finite barrier for nuclear tunnelling at low temperature and by a finite high-temperature activation energy. This process can be due to an activationless ET with the low-temperature rate given by eq IV.20 with $V > 10$ cm^{-1}. Such an electronic coupling can be exhibited, according to eq III.7, for donor–acceptor separations of $R < 6$–7 Å. Such a separation is possible. It should be pointed out, however, that the rate reaction (I.1) is comparable to an even faster than medium-induced VR rates.[28-30] Thus the basic assumption pertaining to the separation of time scales for fast VR and slow ET, expressed in terms of the validity conditions (eq III.2) for the applicability of conventional ET theory, breaks down, and the formalism of sections III and IV does not apply. We are now concerned with a new and interesting physical situation when the assumption of "fast" VR cannot be taken for granted and we have to consider an ET occurring during VR; i.e., we have to treat the competition between ET and VR for this process. This state of affairs can be adequately described in terms of the configurational diagram of Figure 4. We consider two potential surfaces, corresponding to the strong coupling situation, which intersect at x. When the system is initially excited at the energy E_e, it will start from a vibrationally

(34) (a) Clayton, R. K.; Yan, H. F. *Biophys. J.* **1972**, *12*, 867. (b) McElroy, J. D.; Mauzerall, D. C.; Feher, G. *Biochim. Biophys. Acta* **1974**, *333*, 261.

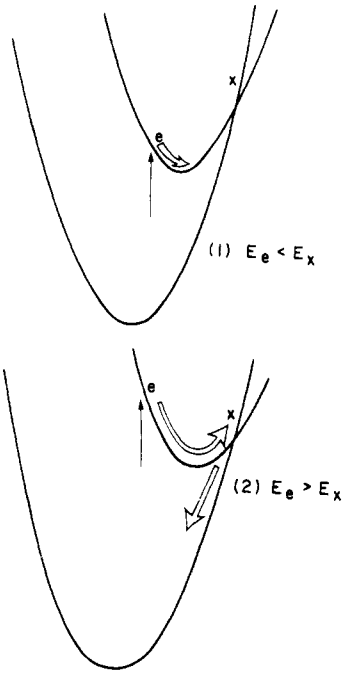

Figure 4. Schematic description of initial excitation followed by vibrational relaxation, which is designated by arrows. When $E_e < E_x$ the system usually equilibrates thermally. When $E_e > E_x$ the system can undergo efficient ET at the crossing point x before equilibration has been accomplished.

excited state to slide downwards by VR. If the initially excited configuration E_e is located below the crossing point E_x, the microscopic ET rates are usually sufficiently low to enable the system to relax vibrationally to a thermally equilibrated configuration from which ET will occur. However, when the initially excited configuration E_e is located above the crossing point E_x, the system will pass on its way downwards through the crossing point of the potential surfaces. At the vicinity of the crossing point the nuclear contribution to the microscopic ET rate is large due to efficient vibrational overlap. Thus, provided that the electronic coupling between the donor and acceptor is reasonably large (i.e., R is not too big), efficient ET will occur at the crossing point. Thus a necessary condition for efficient ET during VR is

$$E_e \geq E_x \tag{V.21}$$

It will be useful at this stage to consider briefly the energetics of the system. The potential surfaces cross at

$$x = (\Delta E + E_S)/\Delta\hbar\omega \tag{V.22}$$

which is characterized by the energy

$$U_{DA}(x) = |\Delta E| + (\Delta E + E_S)^2/4E_S \tag{V.23}$$

for $\Delta E < 0$, which is in accord with eq III.14. Condition V.21 takes the form of (V.24).

$$E_e > |\Delta E| + E_A \tag{V.24}$$

This picture of efficient ET during VR bears a close analogy to the model of Dexter, Klick, and Russell[35] for the quenching of fluorescence in electronic excited states of F center and other ionic centers in solids.[24,36] We propose that the primary ultrafast charge-separation process I.1 occurs from a nonthermally equilibrated nuclear configuration during VR. To explore the dynamics of ET during VR, we shall first consider a semiclassical treatment of the problem utilizing the Landau–Zener (LZ) formalism,[37] which is applicable provided that condition V.21 is satisfied. Subsequently, a quantum mechanical treatment of the competition between ET and VR will be outlined. The purpose of this treatment is not to dwell on formalism but rather to elucidate the physical ingredients which determine the features of these ultrafast ET processes.

(B) Semiclassical Relaxation Model. Consider an idealized model system consisting of harmonic potential surfaces, U_{DA} and $U_{D^+A^-}$, where the anharmonic system medium coupling will be disregarded. The system is excited to the nuclear configuration on the U_{DA} potential surface and starts moving. It will recur through the point x within a period of $2\pi(\omega)^{-1}$. The probability, $\tilde{P}$, for a $DA \rightarrow D^+A^-$ transition per double pass is given by the celebrated LZ formula[37] (V.25),

$$\tilde{P} = 2\exp(-y)[1 - \exp(-y)] \tag{V.25}$$

$$y = 2\pi|V|^2/\hbar v_x|F_{DA} - F_{D^+A^-}| \tag{V.26}$$

where $|V|$ is again the interstate coupling, v_x represents the velocity at x, while $F_j = \partial J_j/\partial q, j = DA$ or D^+A^-, corresponds to the forces at this point. The transition probability (per unit of time) is

$$W = (\omega/2\pi)\tilde{P} \tag{V.27}$$

in the nonadiabatic limit $y \ll 1$ and a second-order perturbation treatment is applicable. In this case

$$W = (\omega/\pi)y \quad y \ll 1 \tag{V.28}$$

while in the adiabatic limit $\gamma \gg 1$ and

$$W = (\omega/\pi)\exp(-y) \quad \gamma \gg 1 \tag{V.29}$$

Returning to our haromine system, we take for the velocity at the crossing point x

$$v_x = [(2/\mu)(E_e - |\Delta E| - E_A)]^{1/2} \tag{V.30}$$

where μ is the effective mass of the oscillator. Note that the velocity is real provided that condition V.24 is obeyed. The difference in the forces at x is

$$|F_{DA} - F_{D^+A^-}| = \hbar\omega\Delta(\mu\omega/\hbar)^{1/2} \tag{V.31}$$

Utilizing eq V.26, V.30, and V.31 we get

$$y = 2\pi|V|^2/\hbar\omega\Delta[2\hbar\omega(E_e - |\Delta E| - E_A)]^{1/2} \tag{V.32}$$

For reasonable order of magnitude estimates of the parameters $V = 10$–$100\ cm^{-1}$, $\hbar\omega = 400\ cm^{-1}$, $\Delta = 10$, and $E_e - |\Delta E| - E_A = 1000\ cm^{-1}$, we get $y \approx 10^{-2}$–10^{-4}. We thus conclude that $y \ll 1$ and the nonadiabatic limit is applicable. The nonadiabatic transition probability is given in terms of V.28 and V.32 and will be written explicitly in the form of eq V.33.

$$W = \frac{2|V|^2}{\hbar\Delta[2\hbar\omega(E_e - |\Delta E| - E_A)]^{1/2}} \tag{V.33}$$

This is the final semiclassical result from ET from nonequilibrium nuclear configurations. Equation V.33 exhibits the following features: (1) W is finite when condition V.24 is obeyed. (2) W diverges when $E_e = E_x$ as expected for the semiclassical model. This nonphysical feature can be amended by a quantum mechanical treatment. (3) For $E_e > E_x$ the rate decreases with increasing E_e, as the velocity at the crossing point increases, making the process less effective. (4) $W \propto \Delta^{-1}$, so that W decreases with increasing the nuclear distortion. (5) $W \propto |V|^2$ is expected for a perturbative result, which is valid as long as $\gamma \ll 1$.

As a rough estimate of W we take the high value of $V = 100\ cm^{-1}$ for the electronic coupling, together with $\hbar\omega = 400\ cm^{-1}$, $E_e - |\Delta E| - E_A = 1000\ cm^{-1}$, and $\Delta = 10$ which results in $W = 4 \times 10^{11}\ s^{-1}$. This calculation should be considered as a rough order of magnitude estimate in view of the approximation inherent in the semiclassical approach. Nevertheless, we can conclude that the mechanism of ET at the crossing of the potential surfaces

(35) Dexter, D. L.; Klick, C. C.; Russell, G. A. *Phys. Rev.* **1955**, *100*, 603.
(36) Bartram, R. H.; Stoneham, A. M. *Solid State Commun.* **1975**, *17*, 1593.
(37) Landau, L. D.; Lifschitz, E. M. "Quantum Mechanics"; Pergamon Press: Oxford, 1960.

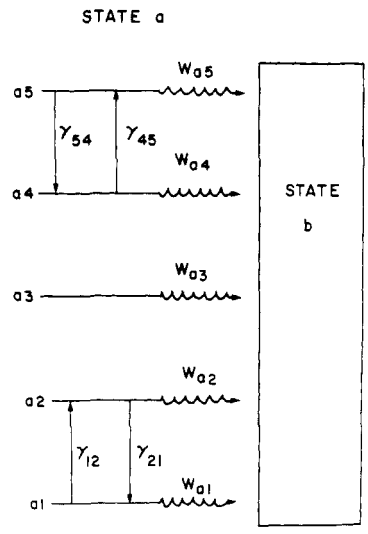

Figure 5. Stochastic model for competition between ET and VR. The microscopic ET rates are W_{av} while $\gamma_{v\to v'}$ denote the *VR* rates.

(provided that V is large) can compete efficiently with VR when the system slides down at the crossing point x.

From this semiclassical analysis two conclusions emerge. First, from the point of view of general methodology, this analysis provided proper justification for the applicability of the nonadiabatic limit. This conclusion provides the basis of the subsequent quantum mechanical treatment. Second, from the practical point of view, the semiclassical model predicts that when condition V.24 is violated, the ET process will be severely retarded. Thus selective optical excitation of the $(BChl)_2$ system will result in efficient ET until the excitation energy will be sufficiently low so that $E_e < E_x$ and then the ultrafast primary ET process will be severely slowed down. The energy dependence of the action spectrum for process I.1 and, in particular, the deviation of this action spectrum from the conventional absorption spectrum of the $(BChl)_2$ dimer will provide a definite proof for the validity of the proposed mechanism for process I.1.

The semiclassical LZ model is grossly oversimplified as it disregards dissipative processes in the system due to anharmonic coupling.[38,24] Furthermore, the vanishing of W at $E_e < E_x$ is a semiclassical result which disregards the effects of nuclear tunnelling. These shortcomings will be overcome by considering a simple quantum mechanical model for the competition between ET and VR.

(C) A Quantum Mechanical Treatment. The problem of coupled ET–VR processes with which we are concerned bears a close analogy to the problem of the occurrence of ultrafast electronic intramolecular radiationless transitions in collisionally perturbed large molecules[39] and to the effects of medium-induced VR on intermolecular electronic energy transfer.[40] Two basic approaches were utilized for the understanding of the effects of VR on the electronic nonradiative process. A quantum mechanical description for the coupled electronic–relaxation–vibrational–relaxation process was advanced[41] which results in rather cumbersome analytical expressions. On the other hand, stochastic models were used.[39,40] The limitation of these stochastic models[39,40] is that they can be solved analytically only for very limited classes of model systems. Nevertheless, stochastic models are extremely useful as they adhere to the chemical intuition and are useful to elucidate the gross features of the coupled ET–VR process.

The stochastic approach assumes that all effects of phase coherence have been eroded in the dense medium; the system is Markovian and devoid of any memory of its past history, so that the dynamics can be adequately described in terms of kinetic master equations for the populations. Figure 5 portrays the relevant kinetic scheme. The states $\{av\}$ of the initial DA manifold exhibit intrastate VR and vibrational excitation processes characterized by the rates $\gamma_{v\to v'}$ as well as interstate *ET*, which is specified by the microscopic ET rates W_{av} (v = 1, 2, ...). The populations p_{av} of the states av are governed by the kinetic equation (V.34)

$$\frac{dp_{av}}{dt} = -\gamma_{v\to v-1}p_{av} - \gamma_{v\to v+1}p_{av} + \gamma_{v+1\to v}p_{a(v+1)} + \gamma_{v-1\to v}p_{a(v-1)} - W_{av}p_{av} \quad \text{(V.34)}$$

with the initial condition (V.35)

$$p_{av}(t = 0) = \delta_{vk} \quad \text{(V.35)}$$

where k is the initially excited state. The total rate, W, of the a → b ET process under nonequilibrium conditions is

$$W = \sum_v W_{av}p_{av} \quad \text{(V.36)}$$

Equations V.34–V.36 constitute the general solution for the problem. Two limiting conditions of the solution are of intrinsic interest. (I) Fast VR: when condition III.5 is satisfied, the populations assume Boltzman equilibrium $p_{av} = \exp(-E_{av}/kT)Z_{av}^{-1}$ with $Z_{av} = \sum_V \exp(-E_{av}/kT)$ and eq V.36 is reduced to the thermally equilibrated muiltiphoton rate given by eq III.5 and III.6. (II) Fast ET from the initially excited state k: when $W_{av} \gg \gamma_{v\to v\pm1}$, the ET occurs essentially from the initially excited state.

For other situations the kinetic equations (V.36) have to be solved numerically by standard procedures. To do so, one has to specify the VR rates as well as the microscopic ET rates. The VR rates can be guessed on the basis of the available experimental data[28-30] to be in the range $\gamma_{v\to v'} \simeq 10^{12}$ s^{-1}. The microscopic ET rates W_{av} occurring from vibrationally excited states of the DA manifold is given by eq III.4a,b. Within the framework of the single-mode approximation the microscopic rates are

$$W_{av} = A\mathrm{FC}(v) \quad \text{(V.37)}$$

where A is given by eq III.11a while FC(v) is the Franck–Condon overlap vibrational nuclear overlap factor between the state v and the state v', which is quasi-degenerate with it, so that

$$\mathrm{FC}(v) = |\langle v|v'\rangle|^2 \quad \text{(V.38)}$$

where $v' = v + |\Delta E|/\hbar\omega$.

For displaced potential surfaces corresponding to DA and to D^+A^- respectively, the Franck–Condon factors (eq V.37) are explicitly given by eq V.39.

$$\mathrm{FC}(v) = |\langle v|v + p\rangle|^2 = \exp(-S)v!(v + p)!\left|\sum_{q=0}^{v}(-1)^{v+p-q}\frac{S^{v+p/2-q}}{q!(v - q)!(v + p - q)!}\right|^2 \quad \text{(V.39)}$$

Equations V.37 and V.39 provide explicit expressions for the microscopic ET rates from an initially excited state v'. Numerical model calculations were preformed for the weak nuclear coupling and for the strong nuclear coupling situations to gain some understanding of the general theoretical dependence of these rates. Typical data for the Franck–Condon factors are presented in Figure 6, which determine the microscopic ET rates according to eq V.37 which for $\hbar\omega$ = 400 cm^{-1} are given by $W_{av} = 3 \times 10^9|V/\mathrm{cm}^{-1}|^2$ s^{-1}. The general features of the microscopic rates are as follows. (a) For $p(0)$ at sufficiently high values of $|\Delta E|$, the exponential energy gap law[42] $p(0) \propto \exp(-\Gamma|\Delta E|)$, with $\Gamma = (\hbar\omega)^{-1} - 2(\hbar\omega)^{-1}$, applies. (b) In the weak and intermediate coupling situations when vertical excitation occurs below the crossing point, then $p(v)$ at a fixed value of ΔE increases roughly exponentially with increasing v. Thus, the rate of the ET is considerably enhanced at a higher excess vibrational energy. (c) When the vertical excitation occurs in the vicinity of the crossing point, the microscopic decay rate, $p(k)$, from the initially excited state k may be large, provided that the electronic coupling V is strong.

(38) Mott, N. F. *Philos. Mag.* **1977**, *36*, 978.
(39) Heller, D. F.; Freed, K. F. *J. Chem. Phys.* **1974**, *61*, 3942.
(40) Kernke, V. N. *Phys. Rev. A* **1977**, *16*, 166.
(41) Nitzan, A.; Jortner, J. *J. Chem. Phys.* **1973**, *58*, 2412.
(42) Englman, R.; Jortner, J. *Mol. Phys.* **1970**, *18*, 145.

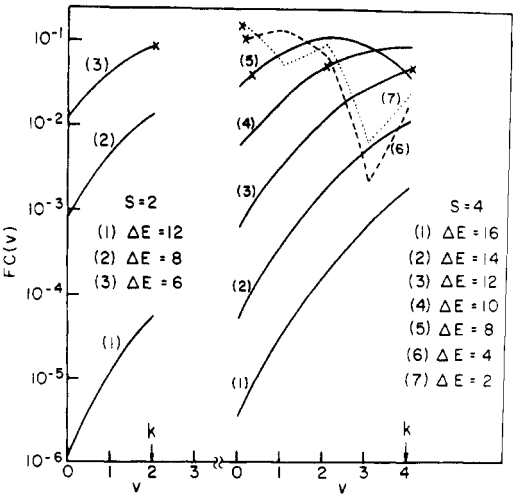

Figure 6. The dependence of the microscopic rates W_{av} for ET on the excess vibrational energy v for several values of the nuclear parameters S and $|\Delta E|$. The initially excited state is k. All energies are presented in units of $\hbar\omega$. The cross represents the crossing point of the point of the partial surfaces and is given wherever it is located below the initially excited state.

When the electronic coupling is in the range $V = 10$–100 cm^{-1}, corresponding to the close spatial proximity of the donor–acceptor pair ($R \simeq 7$–9 Å according to relation III.7), the microscopic ET rates in the vicinity of the crossing X_{ec} of the potential surfaces where FC(v) are $W_{av} \simeq 10^{11}$–10^{13} s^{-1}. Under these circumstances, effective competition between ET and VR will be exhibited. From the foregoing analysis we conclude that the novel mechanism proposed herein of ET during VR will prevail for an exoergic process, provided that the following conditions are satisfied. (1) Intermolecular organization yields short D–A separation, so that $V \sim 10$–100 cm^{-1}. (2) Intramolecular nuclear distortions correspond to an intermediate or strong nuclear coupling, i.e., $S > 1$, so that the crossing point of the two surfaces is not too high. (3) The system is initially excited above the crossing point.

When conditions 1–3 are satisfied, the ET process is characterized by a picosecond or a subpicosecond lifetime as well as by a temperature-independent rate. We propose that the primary charge-separation process (I.1) occurs by this mechanism. As already pointed out in the analysis of the semiclassical rate expression in section V.B, the crucial test for the validity of this mechanism will originate from the study of the dependence of process I.1 on the initial excitation energy. We expect retardation of this ET process when the initial excitation will be moved to lower energies below the crossing point of the two potential surfaces. From the quantum mechanical calculation of the microscopic ET rates presented in Figure 6, it is apparent that the retardation of the ET process, when the excitation energy moves below the crossing point, is gradual rather than abrupt as predicted by the semiclassical model. Optical selection studies inducing process I.1 by direct optical excitation in the $(BChl)_2$ dimer absorption band will be of considerable interest.

VI. Overview of the Charge-Separation Process

We shall attempt to provide a molecular scheme describing the sequence of charge-separation processes as envisioned from the microscopic point of view. We shall consider the intermolecular organization of the donor–acceptor pair which determine the absolute value of the ET rates via the electronic coupling V and to the intramolecular distortions of the donor–acceptor pair which determine the nuclear contributions to the rate. The physical picture is admittedly oversimplified as it rests on the description of intramolecular nuclear contributions in terms of a single-mode picture, while the intermolecular terms V are classified in a crude way according to relation III.7. Nevertheless, this approach will provide a useful scheme for the rationalization of the gross features of charge separation, i.e., the directionality and the specificity of the process, the inefficiency of back-reactions as well as for the magnitude of the ultrafast ET absolute rates, and their temperature independence.

Table I. Energetic Parameters and Configuration Distortions for Potential Surfaces

	j			
	1	2	3	4
$-\Delta E_{jl}$, cm^{-1}	0	6000	8400	9600
Δ_{jl}	0	5.5	2.0	3.5
E_{jl}^{s},[a] cm^{-1}	0	6000	800	2400[b]

[a] $E_{jl}^{s} = (\hbar\omega/2)\Delta_{jl}^2$ with $\hbar\omega = 400$ cm^{-1}. [b] $h\nu = \Delta E_{4l} + E_{jl}^{s} = 12\,000$ cm^{-1} for vertical excitation energy.

We shall consider the charge separation in the reaction center (Figure 1). The intramolecular nuclear contributions are specified in terms of the four one-dimensional potential surfaces (see eq VI.40),

$$U_j(q) = \frac{\hbar\omega}{2}(q - \Delta_{jl})^2 + \Delta E_{jl} \qquad \text{(VI.40)}$$

where the electronic states $j = 1$, 2, 3, and 4 are labeled in the order of increasing energy (eq VI.41).

$$\begin{aligned} j &= 1 \quad (BChl)_2BPhQ \\ j &= 2 \quad (BChl)_2{}^{+}BPhQ^{-} \\ j &= 3 \quad (BChl)_2{}^{+}BPh^{-}Q \\ j &= 4 \quad (BChl)_2{}^{*}BPhQ \end{aligned} \qquad \text{(VI.41)}$$

The characteristic frequency is the molecular frequency of the donor and the acceptor centers corresponding to the nuclear vibrational mode which undergoes large configurational distortion during ET. It is appropriate to take $\hbar\omega = 400$ cm^{-1}.

The energy gaps ΔE_{21}, ΔE_{31}, and ΔE_{32} separating the minima of the potential surfaces are experimentally known.[2] These energetic data were taken from Figure 1 and incorporated in Table I. The energy of the minimum configuration of the curve $j = 4$ is unknown, the only information pertaining to the optical spectrum. In any case, the characteristic frequencies active in the absorption spectrum may be different from those which provide the accepting molecular modes for the ET process. Therefore, the description of the optical absorption of the $(BChl)_2$ dimer in terms of excitation between curves 1 and 4 is quite simple minded. Nevertheless, we have done so, choosing the energy gaps $\Delta E_{41} = 9600$ cm^{-1} and taking $h\nu = 12\,000$ cm^{-1} for the vertical excitation energy. This vertical excitation energy is slightly higher than the experimental vertical excitation energy of the dimer (11 400 cm^{-1}); however, in view of the uncertainty in the one-dimensional picture this approximate choice of $h\nu$ does not modify the basic physical features. To complete the description of the nuclear potential surfaces, we need the equilibrium configurations. Taking $\Delta_{11} = 0$, we have estimated $\Delta_{21} = 5.5$ by assuming that the slow $j = 2 \rightarrow j = 1$ process is activationless. Next, we make use of our proposition that process $j = 3 \rightarrow j = 2$ is activationless. Consequently, making use of condition IV.17, we get $\Delta_{32} = \pm 3.5$ so that we encounter an ambiguous choice of Δ_{31} which can take the values of $\Delta_{31} = 9.0$ or $\Delta_{31} = 2.0$. The possibility $\Delta_{31} = 9.0$ can be eliminated as this large displacement will result in curve crossing between curves $j = 3$ and $j = 1$ at low energies in the vicinity of the minimum of the $(BChl)_2{}^{+}BPh^{-}Q$ nuclear configuration, resulting in an efficient recombination process II.5, which nature avoids. Accordingly, we have taken $\Delta_{31} = 2.0$. Finally, the parameter for Δ_{41} was chosen so that curves $j = 4$ and $j = 3$ intersect above the $j = 1 \rightarrow j = 4$ vertical excitation point. The relevant molecular parameters determining the intramolecular organization are summarized in Table I, while in Table II we summarize the coordinates x and the energies E_x, relative to the ground state $(BChl)_2BPhQ$, calculated from eq V.22 and V.23 for the crossing of the potential surfaces.

Next, we have to consider the intermolecular organization which determines the electronic coupling. The values of V for processes I.1, $4 \rightarrow 3$, I.2, $3 \rightarrow 2$, and I.3, $2 \rightarrow 1$ were estimated in sections IV and V. It is important to make rough estimates of other

Table II. Crossing of Potential Surfaces

(a) Coordinates x (dimensionless)

j				
1	2	3	4	j'
	5.5	11.5	8.5	1
		2.0	0.5	2
			4.5	3
				4

(b) Energies E_x, cm^{-1}

j				
1	2	3	4	j'
	6000	24 400	14 400	1
		8 400	11 600	2
			9 800	3
				4

electronic coupling terms. The electronic coupling for the shortcut reaction (II.4) is expected to be low. We can assert that the electronic coupling responsible for reaction II.4 is similar to that observed for the back-reaction (I.3), i.e., $V_{4\to 2} = V_{2\to 1} \simeq 5 \times 10^{-4}$ cm^{-1}. The electronic coupling for the recombination reaction (II.5) is expected to be large as $V_{3\to 4} = V_{4\to 3} \simeq 10$ cm^{-1}. Finally, we have to consider the residual coupling responsible for the intramolecular radiationless decay process (II.6), which can deactivate the electronically excited state of the dimer. This intramolecular coupling ν is of a different nature than the V which is responsible for intermolecular ET. For internal conversion to the ground state ν originates from the breakdown of the Born–Oppenheimer separability condition and is typically of the order of $\nu \approx 1000$ cm^{-1}.[43] Another decay channel of the singlet electronic excitation can involve intersystem crossing to the triplet state induced by intramolecular spin–orbit coupling.

Figure 7 portrays the potential energy surfaces together with the schematic description of the two initial microscopic processes of charge separation, process I.1 where ET competes with VR at crossing and the activationless process I.2. The recombination process (I.3) occurring in vitro is also indicated. This scheme of intermolecular distortions and intermolecular organization provides an adequate description for the directionality of the charge separation. The efficient exoergic processes (I.1) and (I.2) are driven by large electronic coupling and by proper intramolecular nuclear distortions.

To demonstrate the directionality of the charge separation, we shall show that the reverse uphill processes are negligible. Process II.1, corresponding to the transition $3 \to 4$, is characterized by large electronic coupling $V_{3\to 4} \approx 10$ cm^{-1}. However, this process is endoergic with $\Delta E = 1200$ cm^{-1} and $E_A = 1500$ cm^{-1}. Thus at low temperatures relative to the vibrational frequency, i.e., $k_BT \ll 400$ cm^{-1}, the rate for the $3 \to 4$ reaction is

$$W_{3\to 4} = 2 \times 10^{10} \exp[-1200/(k_BT/cm^{-1})]s^{-1} \quad \text{(VI.42)}$$

being 2×10^5 s^{-1} at 150 K, while at high temperature the rate equation (III.13) is

$$W_{3\to 4} = 1.6 \times 10^{12}(k_BT/cm^{-1})^{-1/2} \exp(-1500/k_BT)\ s^{-1} \quad \text{(VI.43)}$$

being 6×10^7 s^{-1} at 300 K. Obviously, $W_{3\to 4} \ll W_{3\to 2} = 8 \times 10^9$ s^{-1}. Process II.2′ is characterized again by large electronic coupling $V_{2\to 3} \simeq 4$ cm^{-1}. However, once more this process is endoergic with $\Delta E = E_A = 2400$ cm^{-1}. The low-temperature rate is

$$W_{2\to 3} = 8 \times 10^9 \exp[-2400/(k_BT/cm^{-1})]\ s^{-1} \quad \text{(VI.44)}$$

being 0.8 s^{-1} at 150 K, and a high-temperature rate is

$$W_{2\to 3} = 1 \times 10^{11}(k_BT/cm^{-1})^{-1/2} \exp(-2400/k_BT)\ s^{-1} \quad \text{(VI.45)}$$

(43) Parson, W. W.; Clayton, R. K.; Cogdell, R. K. *Biochim. Biophys. Acta* **1975**, *387*, 265.

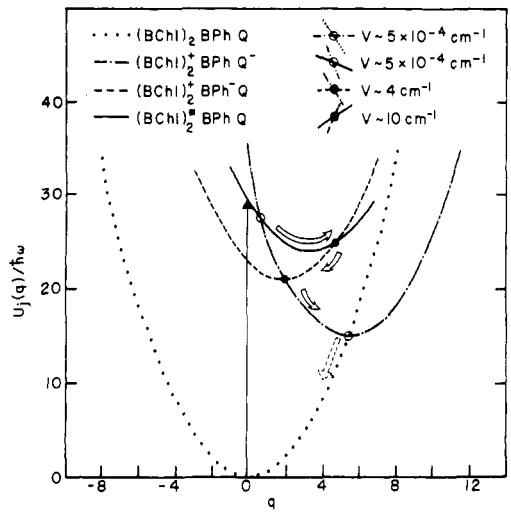

Figure 7. A molecular scheme for the sequence of the microscopic charge-separation processes in bacterial photosynthesis. The four nuclear potential surfaces correspond to the four relative electronic configurations labeled according to eq VI.41. The procedure for the construction of these potential surfaces is described in the text. All energies are normalized to the characteristic frequency $\hbar\omega = 400$ cm^{-1}, while the coordinate is expressed in reduced units. The black dots represent crossing of potential surfaces with efficient electronic coupling V while the open dots denote crossing of pairs of curves characterized by weak V. The vertical arrow represents vertical optical excitation; the two thick arrows denote the pathway of the efficient processes while the broken arrow designates the slow recombination process in vitro.

while assuming the value of 5×10^4 s^{-1} at 300 K. It is apparent that $W_{2\to 3} \ll W_{3\to 2} \simeq 8 \times 10^9$ s^{-1} so that the population of the $(BChl)_2^+BPhQ^-$ potential curve ($j = 2$) will be favored at all temperatures of interest. In vivo this favored $(BChl)_2^+BPhQ^-$ electronic state will accept an electron from cytochrome, resulting in charge separation across the membrane. We conclude that in spite of favorable electronic coupling the back-reactions (II.1′) and (II.2′) are negligible in view of the inefficiency of the endothermic process between nuclear potential surfaces with a moderately large energy gap.

To consider the specificity of the route of the charge-separation process, we have to consider the "shortcut" process (II.5) corresponding to $4 \to 2$ transition. As is apparent from Figure 7 the potential curves 4 and 2 cross below the vertical excitation energy. Nevertheless, the $4 \to 2$ shortcut is blocked by ineffective electronic coupling. The electronic coupling is exceedingly poor, $V_{4\to 2} \simeq 5 \times 10^{-4}$ cm^{-1}, so that the preexponential factor will be low, $A \approx 10^3$ s^{-1}, and the corresponding ET process exceedingly slow on the picosecond time scale of reaction I.1. Accordingly, the branching ratio between process II.5 and reaction I.1 is $\lesssim 10^{-8}$ and the contribution of reaction II.5 is negligible.

Next, we have to discuss the inefficiency of the charge-recombination process (II.5), corresponding to the $3 \to 1$ transition. This process is characterized by large electronic coupling $V \approx 10$ cm^{-1}. However, the nuclear distortions correspond to the moderately weak coupling situation $S = 2$. The nuclear Franck–Condon overlap is extremely unfavorable. To be more quantitative, we express the low-temperature nuclear tunneling rate (eq III.15) in the form $W_{3\to 1} = 1.2 \times 10^{11} \exp(-\gamma p - S)$ s^{-1} with $\gamma = 1.35$, $S = 2$, and $p = 21$, which is $\sim 10^{-3}$ s^{-1} being negligibly small. At high temperatures the $3 \to 1$ rate is characterized by a huge activation energy of 16 000 cm^{-1}, so that this process is ineffective. We thus conclude that the $3 \to 1$ exoergic process is blocked by a large energy gap. The predicted rate $W_{3\to 1}$ is, however, considerably lower than the experimental rate ($\sim 10^7$ s^{-1}) reported[43] for the disappearance of the chlorophyll dimer in the reaction center which involves a reduced quinone. The back-recombination[43] from $(BChl)_2^+BPh^-Q^-$ to the final state $(BChl)_2BPhQ^-$ may involve electron back-transfer via an electronically excited state of the dimer, rather than directly to the ground state. The electronically excited state of the dimer presumably involves a

Table III. Features of the Elementary ET Processes $i \rightarrow j$ ($i,j = 1, 2, 3, 4$) in Bacterial Photosynthesis[a]

i (intial)				
1	2	3	4	j (final)
	exoergic $\lvert\Delta E\rvert = E_S = 6000$ activationless $V \simeq 5 \times 10^{-4}$ slow because of weak V	exoergic $\lvert\Delta E\rvert = 8400$ $E_S = 800$ $V \simeq 10$ blocked by large energy gap	exoergic electronic relaxation $\lvert\Delta E\rvert = 9600$ $\nu \simeq 100$–1000 blocked by large energy gap	1
endoergic $\Delta E = E_A = 6000$ $V \simeq 5 \times 10^{-4}$ blocked by high E_A and low V		exoergic $\lvert\Delta E\rvert = E_S = 2400$ activationless $V \simeq 4$ *efficient*	exoergic curve crossing $V \approx 5 \times 10^{-4}$ blocked by low V	2
endoergic $\Delta E = 8400$ $V \approx 10$ blocked by high E_A	endoergic $\Delta E = E_S = 2400$ $V \approx 4$ blocked by high E_A		ET during VR $V \approx 10$ *efficient*	3
endoergic $\Delta E = 9600$ $\nu \approx 100$–1000 blocked by high E_A	endoergic $\Delta E = 3600$ $E_A = 5400$ $V \approx 5 \times 10^{-4}$ blocked by low V and high E_A	endoergic $\Delta E = 1200$ $E_A = 1400$ $V \simeq 10$ blocked by E_A		4

[a] The energetic parameters ΔE and E_S for the nuclear potential surfaces are expressed in cm^{-1} units; $\Delta E < 0$ for exoergic processes, while $\Delta E > 0$ for endoergic reactions. The electronic coupling V is given in cm^{-1} units.

Table IV. Donor–Acceptor Separations in the Reaction Center

		R, Å	
donor	acceptor	ET theory[a]	magnetic interactions[b]
$(BChl)_2$	BPh	<10	10
BPh	Q	10	10
Q	$(BChl)_2$	20	23

[a] Present work. [b] Reference 45.

triplet state. This problem deserves further study.

Finally, we would like to briefly discuss the inefficiency of the intramolecular radiationless process II.6. The rate of electronic relaxation to the ground state is given by the energy gap law for electronic relaxation[44] $W_{4\rightarrow1} = (2\pi|U|^2/\hbar\langle\omega\rangle)\exp(-S - \gamma p)$, which is analogous to the expressions utilized in the present work for ET. Taking $U = 100$–$1000\ cm^{-1}$, together with $\Delta E = 9600\ cm^{-1}$ ($p = 24$ and $S = 6$), results in $W_{4\rightarrow1} = 8 \times 10^5$–$8 \times 10^7\ s^{-1}$, which is slow on the time scale of the primary charge separation (I.1). We would like, however, to emphasize that in view of extensive theoretical work on intramolecular radiationless transitions[44] the estimate of the internal conversion can serve only as a crude guideline and should not be taken too seriously.

In Table III we have summarized the gross features of the favorable charge separation processes, together with the unfavorable reactions. The general conclusions emerging from our analysis are as follows. (1) The primary charge-separation process (I.1) is driven by large intermolecular electronic coupling V. This reaction occurs from a nonequilibrium nuclear configuration, this pathway being ensured by a proper nuclear intramolecular organization. (2) The second efficient charge-separation process (I.2) is driven by both large intermolecular electronic coupling, due to the spatial proximity of the donor and acceptor centers, and optimal nuclear organization, which leads to an activationless process. (3) To assess the validity of the nuclear coupling terms extracted from the present analysis of reactions I.1, I.2, and I.3, we have assembled in Table IV the donor–acceptor distances, R, extracted in sections IV and V, together with independent structural information, which emerges from the analysis of magnetic interactions.[45] The agreement is as good as can be expected, inspiring confidence in our analysis as well as in the subsequent discussion of some processes which are blocked by small electronic coupling. (4) The directionality of the overall charge-separation processes can adequately be explained by noting that all the endoergic "uphill" processes in the energy ladder, i.e., reactions II.1′ and II.2′, as well as the reaction $2 \rightarrow 4$ are activated, being blocked by a large activation energy, which makes the processes slow on the relevant time scale. (5) The specificity of the charge-separation process, which occurs "downhill" on the energy ladder, is ensured as the shortcut reaction II.4 and is blocked by a small electronic coupling, i.e., by unfavorable structural organization of the donor and acceptor centers. (6) The inefficiency of the charge recombination from P^+I^-X to the ground state, due to the exoergic reaction $3 \rightarrow 1$, is implied by a large energy gap which, according to eq IV.15, results in an exponential decrease of the ET probability for large values of p. This conclusion concerning the $3 \rightarrow 1$ process implies that the back-recombination in the reaction center involving X^-,[43] occurring on the time scale of 10 ns,[43] involves an electronically excited configuration. (7) The inefficiency of the charge-recombination process (I.3) in vivo on the time scale of the reduction of $(BChl)_2^+$ by cytochrome c is implied by weak electronic coupling.[18] (8) Electronic relaxation of the excited state $(BChl)_2^+$ on the relevant (picosecond) ultrashort time scale is blamed on a sufficiently large electronic energy gap.

From the foregoing analysis it is apparent that the dynamics of the primary events of charge separation is determined by the interplay between the following ingredients: (a) dynamic effects of competition between ultrafast ET and vibrational relaxation; (b) intermolecular organization, which determines the electronic coupling; (c) intramolecular distortions, originating from intermolecular nuclear configurational changes.

These effects combine in driving the charge-separation process in the proper direction, ensuring the proper biological utilization of the excitation energy in the reaction center.

Acknowledgment. I am indebted to Dr. P. M. Rentzepis and to Professor R. Bersohm for stimulating and thought-provoking discussions. I wish to thank Dr. P. L. Dutton for an interesting discussion of his magnetic data. Thanks are due to Professor J. J. Hopfield for his comments on the manuscript. I am grateful to Ephraim Buhks for his help in the numerical calculations.

(44) Jortner, J.; Mukamel, S. *MTP Int. Rev. Sci.: Phys. Chem., Ser. Two* **1975**, 329.

(45) Tiede, D. M.; Leigh, J. S.; Dutton, L. *Biochim. Biophys. Acta* **1978**, *503*, 524.